2014

Array of Surface-Confined Glow Discharges in Atmospheric Pressure Helium: Modes and Dynamics

D. Li

D. X. Liu

Q. Y. Nie

H. P. Li

H. L. Chen

See next page for additional authors

Original Publication Citation

Li, D., Liu, D. X., Nie, Q. Y., Li, H. P., Chen, H. L., & Kong, M. G. (2014). Array of surface-confined glow discharges in atmospheric pressure helium: Modes and dynamics. *Applied Physics Letters*, *104*(20), 1-5, Article 204101. https://doi.org/10.1063/1.4878505

Array of surface-confined glow discharges in atmospheric pressure helium: Modes and dynamics

D. Li,[1] D. X. Liu,[1,a)] Q. Y. Nie,[2] H. P. Li,[2] H. L. Chen,[3] and M. G. Kong[1,3,4,a)]
[1]*Center for Plasma Biomedicine, State Key Laboratory of Electrical Insulation and Power Equipment, Xi'an Jiaotong University, Shaanxi, People's Republic of China*
[2]*Department of Engineering Physics, Tsinghua University, Beijing 100084, People's Republic of China*
[3]*Frank Reidy Center for Bioelectrics, Old Dominion University, Norfolk, Virginia 23508, USA*
[4]*Department of Electrical and Computer Engineering, Old Dominion University, Norfolk, Virginia 23529, USA*

(Received 23 March 2014; accepted 3 May 2014; published online 20 May 2014)

Array of atmospheric pressure surface discharges confined by a two-dimensional hexagon electrode mesh is studied for its discharge modes and temporal evolution so as to a theoretical underpinning to their growing applications in medicine, aerodynamic control, and environmental remediation. Helium plasma surface-confined by one hexagon-shaped rim electrode is shown to evolve from a Townsend mode to a normal and abnormal glow mode, and its evolution develops from the rim electrodes as six individual microdischarges merging in the middle of the hexagon mesh element. Within one hexagon element, microdischarges remain largely static with the mesh electrode being the instantaneous cathode, but move towards the hexagon center when the electrode is the instantaneous anode. On the entire array electrode surface, plasma ignition is found to beat an unspecific hexagon element and then spreads to ignite surrounding hexagon elements. The spreading of microdischarges is in the form of an expanding circle at a speed of about 3×10^4 m/s, and their quenching starts in the location of the initial plasma ignition. Plasma modes influence how input electrical power is used to generate and accelerate electrons and as such the reaction chemistry, whereas plasma dynamics are central to understand and control plasma instabilities. The present study provides an important aspect of plasma physics of the atmospheric surface-confined discharge array and a theoretical underpinning to its future technological innovation. [http://dx.doi.org/10.1063/1.4878505]

Large-area atmospheric pressure gas discharges have recently received growing interest for their use in numerous applications of societal significance, for example, biomedicine, aerodynamic flow control, environment remediation, and nanostructure fabrication.[1,2] Three desirable plasma features are common for most applications, namely, ambient air operation, near ambient temperature, and plasma homogeneity over a large surface area of hundreds square centimeters. Yet ambient air plasmas are characteristically in the spatially inhomogeneous modes of coronas and sparks, and the homogeneous glow mode appears, when existing, in a narrow parametric space.[3] This stems from the fact that the electron mean-free path of atmospheric plasmas is less than one micron,[4] and so plasma instabilities such as glow-to-arc instabilities can develop from a tiny micron-scale area where particle collisions are very frequent already and where effective control is needed. In addition to spatial homogeneity, the glow mode is desirable also because a larger proportion of its input electrical power density is used for electron production than its corona and spark counterparts. Its electron kinetics may be more effectively controlled for superior application efficacy.[5,6]

A common technique for achieving glow-like discharges is to use a comb of surface-mount strip electrodes with a long and narrow air gap between two adjacent electrode strips. Spread of plasma instabilities is restricted in the direction of the narrow width of the long air gap, and so essentially the strip electrode structure provides a one-dimensional control of plasma instabilities to alleviate the difficulty of achieving plasma homogeneity over a large surface.[7–10] Existence of the glow mode is yet to be reported for such surface discharges and plasma images published appear to typically contain numerous corona microdischarges along the edge of each electrode strip. For a greater spatial confinement of plasma stabilities, a recent advance is to use a mesh electrode with each mesh element having a closed rim electrode, thus enabling a two-dimensional restriction to the spreading of possible plasma instabilities.[11] Each mesh element is square shaped, and the resulting surface plasma is essentially an array of similar surface-microplasmas each of sub-millimeter squared.[11] So far, the benefits of such surface microplasmas array have been shown in terms of its efficacy in biology applications[11] and its reaction chemistry.[12] Many important features of their plasma physics including possible existence of the glow mode have not been reported so far, and this is the motivation of the present study.

In this study, we consider a surface microdischarge array with a hexagon-shaped mesh electrode. Figure 1 shows (a) a schematic of the experiment setup and (b) a typical image of an array of surface microdischarges in atmospheric pressure helium. The mesh electrode was made from stainless steel and served as the ground electrode, and the counter electrode was

[a)]Authors to whom correspondence should be addressed. Electronic addresses: liudingxin@gmail.com and mglin5g@gmail.com

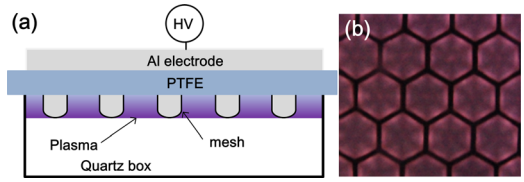

FIG. 1. Array of surface-confined plasmas with (a) its electrode unit; (b) $2.4 \times 2.4\ \text{cm}^2$ area of an end-on image in atmospheric helium.

an aluminum plate of $4 \times 4\ \text{cm}^2$ connected to the high voltage (HV) terminal of a sinusoidal power supply. The two electrodes sandwiched a polytetrafluroethene (PTFE) plate of 1 mm in thickness and a lager surface area than the electrode area to avoid flashover discharges. Each mesh element had a closed rim electrode having a hexagon shape with the distance between two parallel sides being 6 mm, and the electrode rim had a width of 760 μm and a thickness of 550 μm. The mesh density is about 3.2 meshes/cm^2. The excitation frequency was 20 kHz at which the glow mode was difficult to achieve in air and as such helium was used in this study. To control the gas environment, the electrode unit was housed inside a quartz box of $6 \times 4 \times 4\ \text{cm}^3$ through which helium (5N) was fed at a flow rate of 5 l/min. The applied voltage was measured with an HV-probe and the discharge current was obtained by measuring the voltage across a small resistor in series with the grounded electrode. Fast plasma images were obtained with an ICCD camera.

Ignition of the surface microdischarge array was at a peak-to-peak applied voltage of $V_{pp} = 1.44$ kV, at which the plasma appeared only in one or two hexagon elements, and an increase in V_{pp} to above 1.81 kV led to the microplasmas spreading over the entire electrode. Stable plasma conditions were found for 1.8–11.0 kV. Figure 1(b) was obtained at $V_{pp} = 7$ kV and with an exposure time of 1/16 s. It is evident that each microdischarge has a distinct structure with intense emission along the rim electrode. The brightest of the intense emission region is near the middle of a (straight) side electrode. An electrostatics simulation found that the largest electric field is indeed around the middle of each side of a hexagon rim electrode.

Voltage and discharge current of the surface microdischarge array are shown as a function of time in Figure 2(a) at $V_{pp} = 7$ kV. There are six current peaks in the positive cycle of the applied voltage and three current peaks in the negative cycle. The discharge current density is up to 3.8 mA/cm^2. The current pulsewidth is 0.6–1.1 μs in the positive half cycle and 2.2–3.6 μs in the negative half cycle. The interval time between two consecutive current peaks is longer in the negative half cycle. It is clear that the discharge events in the two half voltage cycles are different. This asymmetry is distinct from a conventional dielectric barrier discharge (DBD) between two parallel plate electrodes. The first three positive current pulses and the three negative current pulses of Figure 2(a) are marked in the Lissajous figure in Figure 2(b), from which the net charge transferred during the first three positive current pulses was found to be 13.8 nC, 10.8 nC, 10.7 nC and the net transferred charge in the negative cycle was 18.5 nC, 15.6 nC, 15.3 nC, respectively. The large amounts of the transferred charges in the negative half cycle are consistent with the larger pulsewidth of the

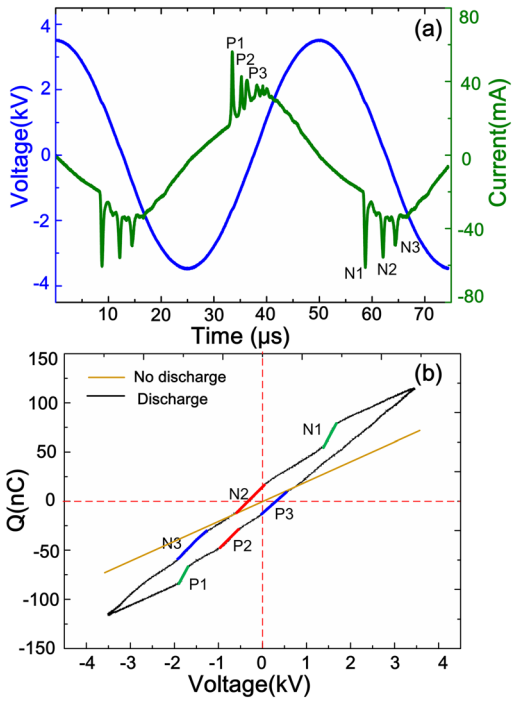

FIG. 2. (a) Waveforms of the applied voltage and the discharge current at $V_{pp} = 7$ kV, and (b) is corresponding Lissajous figure.

corresponding current pulses. From the Lissajous figure, it was also found that the total capacitance of the electrode unit is 16 pF and the averaged power density is 0.29 W/cm^2 or 5.3 W/cm^3 with the plasma thickness approximated by the mesh thickness of 550 μm, about one order of magnitude above those of conventional atmospheric helium DBDs.[13–15] It is worth mentioning that current oscillations in Figure 2(a) are common in dielectric barrier discharges and are often due to electrical charging and discharging of the dielectric barriers and possibly localized microdischarges.[16] The waveform of current oscillations is similar to that of barrier free plasmas at reduced gas pressures with the latter induced largely by relaxation of the electric current in the closed circuit loop.[17]

Dissipated electrical power density is shown in Figure 3 as a function of the peak-to-peak voltage. The microdischarges were found to be temporally stable and spatially homogenous with the greatest optical emission in a thin layer

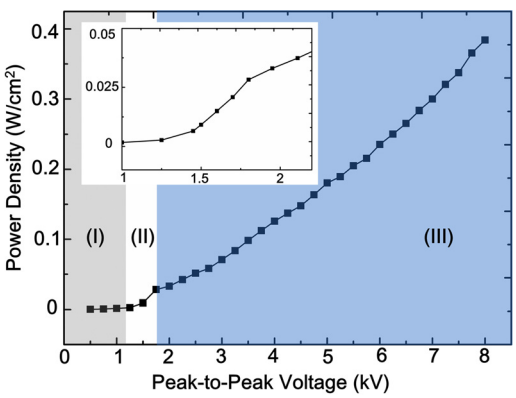

FIG. 3. Applied voltage dependence of the dissipated power with region I being without plasma, II being in the normal glow mode, and III being in the abnormal glow. The bounds of normal glow region are 1.44 kV and 1.81 kV.

region along the electrode edge for $V_{pp} > 1.44$ kV (data not shown). For $V_{pp} = 1.44$–1.81 kV (region II in Figure 3), the microdischarges covered only part of the 4×4 cm^2 electrode area. The discharge current was found to increase with the applied voltage but with an approximately constant current density, distinct features of the normal glow mode. For $V_{pp} = 1.81$–8.0 kV (region III in Figure 3), the plasma now covered the entire electrode area and both the discharge current and the current density increased with the applied voltage. This is an abnormal glow discharge.[18–20] To see dynamic evolution of a single microdischarge, imaging with an exposure time of 100 ns was taken during the main current pulses in the positive and the negative half cycles as shown in Figure 4 for $V_{pp} = 7$ kV. There is a distinct difference in the plasma structure for the two half voltage cycles, continuing the asymmetry in the current and the charge in Figure 2. In the positive half cycle, the region of the greatest emission is much closer to the edge of the electrode and is static. The emission intensity is higher than the negative half cycle as the mesh electrode is the instantaneous cathode during the positive half cycle. As the mesh electrode is naked without dielectric insulation, it supports secondary electron emission and a strong electric field in the sheath region for stronger ionization when it is the instantaneous cathode.[21]

The structure of the microdischarge is seen to evolve intriguingly from the first to the last current pulse (i.e., the first to the last individual discharge events) within the same half cycle. In the positive half cycle, the microdischarge produced in the first current pulse is seen to evolve from a weak plasma in P1(a), through a very strong plasma in P1(c), and finally to a weak plasma in P1(e) and this rise-and-fall repeats in all six discharge events in Figures 4(c) and 4(d). The strongest discharge at P1(c) has six narrow and long regions of bright emission, and each such emission region is close to its nearest side electrode and centered to the middle of the side electrode where the largest plasma-free electric field is found. This general pattern is also evident in the five plasma images for P3. However, for P2, there are two strong emission regions on each electrode side and these two emission regions are now off the center of the side electrode. This indicates that two electric field maxima are now established on each side electrode, caused by the space-charge electric field of the charges on the PTFE surface. Charges released from the first discharge event of P1 are likely to be deposited near the center of one side electrode. The deposited charges set up an electric field in the opposing direction to the direction of the applied voltage, thus reducing the overall local electric field near the center of the side electrode. As a result, the second discharge event is initiated away from the center of the side electrode and in this case there are two simultaneous discharge events off the center of the electrode side. Following the same principle, the third discharge event is initiated away from the centers of the previous discharge events and is now located in the midpoint between the previous two discharge centers. The above process is a self-organization caused by dynamic change of the deposited charges within a confined hexagon space.

In the negative half cycle, when the mesh electrode is the instantaneous anode, the plasma is initiated from near the electrodes and then moving away from the electrode. The movement velocity is highest at 5×10^3 m/s for the first current pulse and 2.1×10^3 m/s for the third pulse. Here, the most negative potential on the PTFE surface is at the center of the hexagon, and it acts as a virtual cathode. Therefore, the movement of the light emission region is cathode-directed. The cathode-directed movement leaves behind positive charges being deposited near the electrode thus enhancing the electric field at the virtual cathode and supporting a significant emission there (see N2(c)).

A closer look at the plasma structure of the first positive current pulse at P1(c) is shown in Figure 5. It has all the structural hallmark of a glow discharge with Aston dark space, negative glow, Faraday dark space, and positive column placed away from the instantaneous cathode progressively.[13,21–23] The thickness of the sheath between the electrode and the negative glow is about 40 μm, much smaller than that in DBDs in narrow atmospheric helium

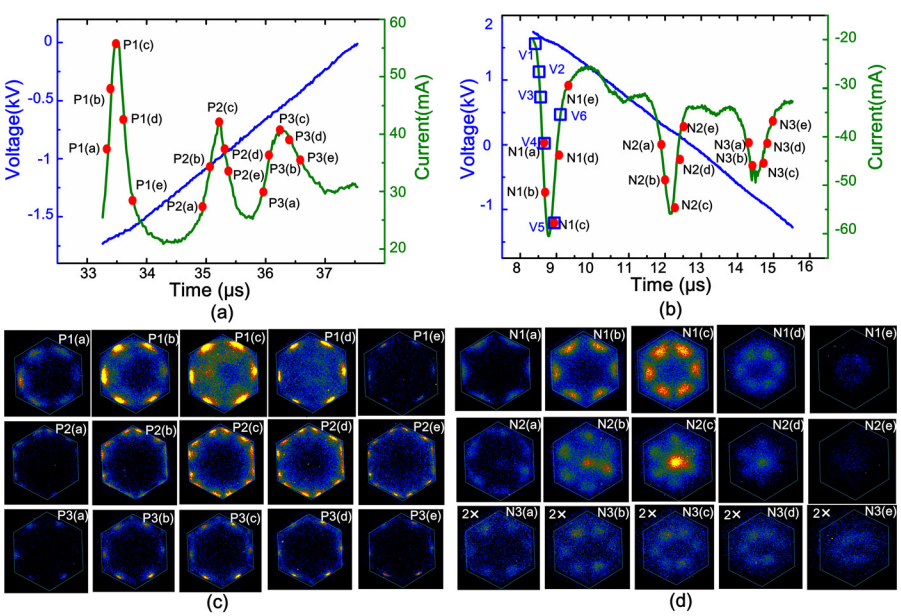

FIG. 4. Current-voltage characteristics during the first three discharge events in (a) the positive half-cycle and (b) the negative half cycle, in which the instants of the iCCD images are marked with P_m(a)–P_m(e) and N_m(a)–N_m(e) for the positive and negative half cycles, respectively. Here, $m = 1$–3 for the 1st, 2nd, and 3rd current pulses. Dynamic evolution of the plasma structure is shown in nanosecond images (exposure time = 100 ns) for (c) the positive half cycle and (d) the negative half cycle. The emission intensity is too weak for N_3(a)–N_3(e) and so is multiplied by a factor of two.

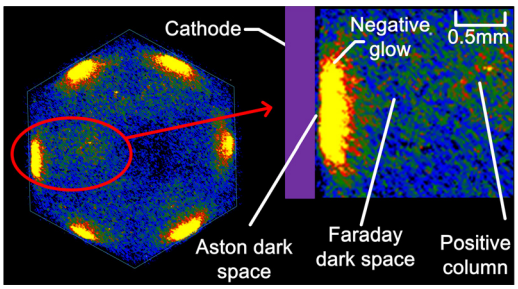

FIG. 5. Plasma structure of a glow discharge during the first positive current pulse.

gap. The strong emission region has a length of ~1.5 cm, much larger than the size of a corona discharge. Images of weaker plasmas (e.g., those at P2(a) and N2(a)) are typical of Townsend discharges. Figures 4(c) and 4(d) show plasma evolution in Townsend and glow modes. Townsend and glow modes shown in Figures 4 and 5 are similar to those observed without dielectric barriers at reduced gas pressures[18,19] and those with dielectric barriers at atmospheric pressure.[20,24]

An interesting phenomenon is the propagation of an ignited microdischarge to nearby mesh elements that are yet to be ignited. To show this clearly, nanosecond images of the entire microdischarge array are taken at six instants of the first negative current pulse (point V1–V6 in Figure 4(b)) and are shown in Figure 6. Images at V1 to V4 show a circular region of ignited microdischarges and its progressive expanding. The expanding circle remains centered at the origin of the initial circle at V1, and at V4 a second smaller circle appears. These two circles of ignited microdischarges merge at just before V5 when the entire electrode is now covered with microdischarges. Subsequently, the microdischarges centered around the original circle (at V1) start to quench as shown in V6. The time scale from V1 to V5 is about 400 ns, and the spreading speed of the light emission was found to be 2.86×10^4 m/s. The propagation of microdischarges has similarities to that in a cavity plasma array in argon/neon,[25] though the latter having a lower speed of 3×10^3/s. It is noted that the formation of an individual microdischarge in its mesh hexagon starts with a partial light-emitting hexagon (see V2, for example). To see how quickly the appearance of a given plasma structure hops from one mesh hexagon to another, we use the sheath thickness, d_s, as a measure of the stage of a glow discharge within a fully lit hexagon. At V4, $d_s \approx 500\,\mu$m at location A and $d_s < 500\,\mu$m at location B. As the time of V5, the sheath thickness at location B is now 500 μm (and that at A is larger than 500 μm). So a glow discharge structure defined with $d_s = 500\,\mu$m sheath thickness is seen at location A at V4 and the same glow structure appears at location B at V5. The appearance-hoping speed (3.8×10^4 m/s) is similar to the propagation speed of ignited microdischarges.

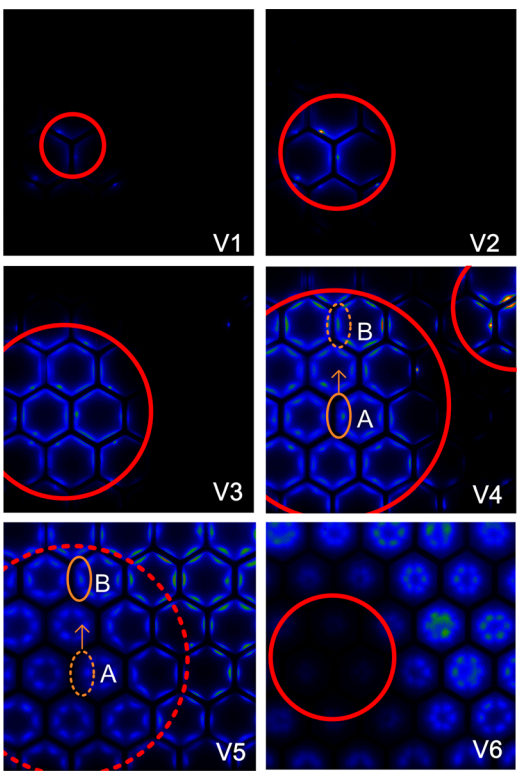

FIG. 6. Spreading and propagation of the microdischarges at six instants (V1–V6) of the first negative current pulses in Figure 4. Exposure time = 100 ns.

One question is whether the appearance and disappearance of the microdischarges in Figure 6 may lead to a large sample being treated more in one location than the other. Assuming a square sample of $20 \times 20\,\text{cm}^2$, the time taken from one corner to its diagonal corner is about 0.099 s, much shorter than the typical treatment time of minutes in plasma medicine.

In conclusion, the array of surface-confined microdischarges was characterized in terms of its electrical properties, its modes, and its dynamic evolution within one mesh hexagon and on the entire electrode. Its characteristics appear well suited for biomedical and other applications of atmospheric pressure plasmas, and for large area applications such surface-confined microdischarge arrays offer an alternative to two other atmospheric pressure plasma array technologies, namely, the cavity-confined microdischarge array[25–27] and the atmospheric pressure plasma jet array.[28–30] Details of plasma modes and their dynamics offer opportunities to tailor-design the surface microdischarge array and to extend the technology for wider operating conditions.

This work was supported by the National Science Foundation of China (Grant Nos. 51307134 and 51221005).

[1]M. G. Kong, G. Kroesen, G. Morfill, T. Nosenko, T. Shimizu, J. van Dijk, and J. L. Zimmermann, New J. Phys. **11**, 115012 (2009).
[2]H. E. Wagner, R. Brandenburg, K. V. Kozlov, A. Sonnenfeld, P. Michel, and J. F. Behnke, Vacuum **71**, 417 (2003).
[3]Y. Akishev, M. Grushin, I. Kochetov, V. Karal'nik, A. Napartovich, and N. Trushkin, Plasma Sources Sci. Technol. **14**, S18 (2005).
[4]F. Iza, G. J. Kim, S. M. Lee, J. K. Lee, J. L. Walsh, Y. T. Zhang, and M. G. Kong, Plasma Processes Polym. **5**, 322 (2008).
[5]S. Guimond and M. R. Wertheimer, J. Appl. Polym. **94**, 1291 (2004).
[6]D. Z. Pai, D. A. Lacoste, and C. O. Laux, J. Appl. Phys. **107**, 093303 (2010).
[7]M. Simor, J. Rahel, P. Vojtek, M. Cernak, and A. Brablec, Appl. Phys. Lett. **81**, 2716 (2002).
[8]J. Pons, E. Moreau, and G. Touchard, J. Phys. D: Appl. Phys. **38**, 3635 (2005).
[9]J. M. Williamson, D. D. Trump, P. Bletzinger, and B. N. Ganguly, J. Phys. D: Appl. Phys. **39**, 4400 (2006).

[10]S. Pekarek, J. Phys. D: Appl. Phys. **45**, 075201 (2012).
[11]G. E. Morfill, T. Shimizu, B. Steffes, and H.-U. Schmidt, New J. Phys. **11**, 115019 (2009).
[12]Y. Sakiyama and D. B. Graves, Plasma Sources Sci. Technol. **22**, 012003 (2013).
[13]F. Massines, A. Rabehi, P. Decomps, R. B. Gadri, P. Segur, and C. Mayoux, J. Appl. Phys. **83**, 2950 (1998).
[14]M. G. Kong and X. T. Deng, IEEE Trans. Plasma Sci. **31**, 7 (2003).
[15]H. Luo, Z. Liang, B. Lv, X. Wang, Z. Guan, and L. Wang, Appl. Phys. Lett. **91**, 221504 (2007).
[16]F. Massines, N. Gherardi, N. Naude, and P. Segur, Eur. Phys. J. Appl. Phys. **47**, 22805 (2009).
[17]A. V. Phelps, Z. Lj. Petrovic, and B. M. Jelenkovic, Phys. Rev. E **47**, 2825 (1993).
[18]Z. Lj. Petrovic and A. V. Phelps, Phys. Rev. E **56**, 5920 (1997).
[19]E. Wagenaars, M. D. Bowden, and G. M. W. Kroesen, Plasma Sources Sci. Technol. **14**, 342 (2005).
[20]J. J. Shi, D. W. Liu, and M. G. Kong, Appl. Phys. Lett. **89**, 081502 (2006).
[21]J. J. Shi and M. G. Kong, J. Appl. Phys. **94**, 5504 (2003).
[22]S. Y. Moon, J. K. Rhee, D. B. Kim, and W. Choi, Phys. Plasma **13**, 033502 (2006).
[23]J. L. Walsh, F. Iza, N. B. Janson, V. J. Law, and M. G. Kong, J. Phys. D: Appl. Phys. **43**, 075201 (2010).
[24]J. J. Shi, J. Zhang, G. Qiu, J. L. Walsh, and M. G. Kong, Appl. Phys. Lett. **93**, 041502 (2008).
[25]J. Waskoenig, D. O'Connell, V. Schulz-von der Gathen, J. Winter, S.-J. Park, and J. G. Eden, Appl. Phys. Lett. **92**, 101503 (2008).
[26]S. J. Park, J. Chen, C. Liu, and J. G. Eden, Appl. Phys. Lett. **78**, 419 (2001).
[27]J. G. Eden, S. J. Park, N. P. Ostrom, and K. F. Chen, J. Phys. D: Appl. Phys. **38**, 1644 (2005).
[28]Z. Cao, J. L. Walsh, and M. G. Kong, Appl. Phys. Lett. **94**, 021501 (2009).
[29]Z. Cao, Q. Nie, D. L. Bayliss, J. L. Walsh, C. S. Ren, D. Z. Wang, and M. G. Kong, Plasma Sources Sci. Technol. **19**, 025003 (2010).
[30]J. Y. Kim, J. Ballato, and S. O. Kim, Plasma Processes Polym. **9**, 253 (2012).